

5. A. Cappy, Noise modeling and measurement techniques, IEEE Trans Microwave Theory Tech 36 (1988), 1–10.
6. J.I. Alonso, B.P. Dorta, C. Crespo, and F. Pérez, Commercial balanced optical front-end for 2.5 Gbit/s continuous phase frequency shift keying (CPFSK) coherent transmission system, Fiber Opt Network Components, Amsterdam, The Netherlands, Mar. 1995, SPIE 2449, pp. 142–151.
7. P. Dorta, C. Crespo, F. Pérez, and J.I. Alonso, Modeling of commercial p-i-n photodiodes and optimization of optical-electrical interfaces in balanced receivers, Topical Meeting Opt Microwave Interactions, Nov. 1994, pp. 155–158.

© 2000 John Wiley & Sons, Inc.

## CHARACTERIZATION OF A THREE-DIMENSIONAL ETCHED-GROOVE SEPARATION OF ADJACENT OPTICAL WAVEGUIDES

Husain M. Masoudi<sup>1</sup>

<sup>1</sup> Department of Electrical Engineering  
King Fahd University of Petroleum and Minerals  
Dhahran, Saudi Arabia

Received 5 April 2000

**ABSTRACT:** A technique for inhibiting the optical channel interaction between two waveguides of a three-dimensional directional coupler structure is investigated. The technique, which uses an etched groove (slot) in the space between the channels, proved to be much more effective compared to the classical method of bending the waveguides away from each other to terminate interaction. Using the three-dimensional explicit finite-difference beam-propagation method, the characteristic parameters of the etched groove have been studied carefully to find the optimum case. We also show that the application of the groove is always accompanied by a small radiation power loss. © 2000 John Wiley & Sons, Inc. Microwave Opt Technol Lett 26: 385–390, 2000.

**Key words:** optical waveguides; integrated optics; grooves; beam propagation

### 1. INTRODUCTION

Many integrated optical elements, such as switches, modulators, and directional couplers, depend, in their operation of optical processing, on the interaction of optical beams between two adjacent waveguides. Usually, these devices are designed such that the interaction takes place on a precise engineered length. After that, the interaction between the two waveguides is to be terminated. In most cases, the two waveguides are bent away from each other to minimize the coupling effect, which is inversely proportional to the distance between the two channels. This method is not effective because it wastes a lateral space of the device substrate due to the bending action. In addition, the technique does not immediately end the interaction between the two waveguides, and sometimes it is accompanied by substantial power loss. An alternative technique for the isolation of waveguide interactions is the introduction of an abrupt etched groove (slot) in the space between the channels. The method showed its effectiveness in 2-D using slab waveguide models [1].

In this work, the characterization of three-dimensional channel isolation using the etched groove technique is shown. We show the full analysis of the technique by addressing the variation of the three important parameters that optimize

channel isolation using an etched groove, which are the depth, width, and location of the groove. Contrary to the belief that a symmetrical etched groove produces optimum results [2], it is shown in the present work that an asymmetric etched groove can inhibit the interaction more abruptly with little power loss. We use the three-dimensional explicit finite-difference beam-propagation method (EFD-BPM) to follow the propagation of an optical beam in a three-dimensional directional coupler structure made of two dielectric rib waveguides. The EFD-BPM is found to be very suitable for the problem at hand; in addition, it is simple and highly efficient [4–5].

### 2. NUMERICAL METHOD

We start with the scalar parabolic equation for a three-dimensional field  $\phi$ :

$$2jk_o n_o \frac{\partial \phi}{\partial z} = \frac{\partial^2 \phi}{\partial x^2} + \frac{\partial^2 \phi}{\partial y^2} + k_o^2 (n^2 - n_o^2) \phi \quad (1)$$

where  $n_o$  is a reference refractive index,  $k_o$  is the free-space wavenumber, and  $n(x, y, z)$  is the refractive index. We use the central finite-difference approximation for the partial derivatives acting on the field  $\phi$  in Eq. (1) as

$$\frac{\partial^2 \phi(\rho, z)}{\partial \rho^2} = \frac{\phi(\rho + \Delta\rho, z) - 2\phi(\rho, z) + \phi(\rho - \Delta\rho, z)}{\Delta\rho^2} \quad (\rho = x, y)$$

$$\frac{\partial \phi(\rho, z)}{\partial z} = \frac{\phi(\rho, z + \Delta z) - \phi(\rho, z - \Delta z)}{2\Delta z} \quad (2)$$

where  $\Delta\rho$  and  $\Delta z$  are the transverse mesh size and the longitudinal step size of the field, respectively. Then the EFD-BPM algorithm can be obtained as [3–5]

$$\phi_{i,m}(z + \Delta z) = \phi_{i,m}(z - \Delta z) + a_x [\phi_{i-1,m}(z) + \phi_{i+1,m}(z)] + a_y [\phi_{i,m-1}(z) + \phi_{i,m+1}(z)] + b_{i,m} \phi_{i,m}(z) \quad (3)$$

where

$$b_{i,m} = \left( \frac{\Delta z}{jk_o n_o} \right) \left[ k_o^2 (n_{i,m}^2 - n_o^2) - \frac{2}{\Delta x^2} - \frac{2}{\Delta y^2} \right],$$

$$a_x = \frac{\Delta z}{(jk_o n_o \Delta x^2)}, \text{ and } a_y = \frac{\Delta z}{(jk_o n_o \Delta y^2)}$$

which is second-order accurate with respect to  $z$ .  $i$  and  $m$  represent the discretization of the transverse coordinates  $x$  and  $y$ , respectively. Equation (2) is stable under the following condition [3]:

$$\Delta z < 2k_o n_o \left[ \frac{4}{\Delta x^2} + \frac{4}{\Delta y^2} + k_o^2 |n_{i,m}^2 - n_o^2|_{\max} \right]^{-1}.$$

On the other hand, the EFD-BPM in Eq. (3) is very efficient because marching the input field one propagational step requires multiplication with a very sparse matrix that contains

only five nonzero elements in each row [3–5]. In addition, the method proved to be very useful in modeling long 3-D optical devices using parallel computers, and this is due to the high efficiency of the algorithm when implemented in the parallel environment [4–5].

### 3. RESULTS AND DISCUSSIONS

For the purpose of studying the effect of an etched-groove separation of adjacent optical waveguides, a three-dimensional dielectric rib-waveguide directional coupler structure is used. Figure 1(a) shows a cross-sectional view of the structure, with an etched groove designed between the two arms of the waveguides. The first guided mode, shown in Figure 1(b), of the isolated rib waveguide is used as input in all computations. The power spectral method has been used to compute the mode-effective index and the field distribution of the first guided mode from the BPM field [6]. This method uses the numerical correlation function, between an input

field (Gaussian field in this case) and the BPM field, to locate the peaks in the Fourier space. First, the correlation is multiplied by a Hanning window function, and then Fourier transformation is performed with respect to the axial distance  $z$ . The position of the power spectral peaks can determine, by applying a line-shape fitting technique, the parabolic propagation constant from which the Helmholtz propagation constant can be computed. The full description of the power spectral method can be found in [6]. In addition, the coupling length of the directional coupler structure of Figure 1(a), without an etched groove ( $D_g = 0$ ), is calculated using the spectral method [4]. In order to excite the even super mode, the sum of two equal-amplitude Gaussian fields centered in the middle of each arm of the coupler has been launched as an input. The same has been done to excite the odd super mode of the coupler, except that the two Gaussian fields have the opposite sign [4]. Calculating the super mode effective indexes of the even ( $n_e^{eff}$ ) and odd ( $n_o^{eff}$ ) modes, then the

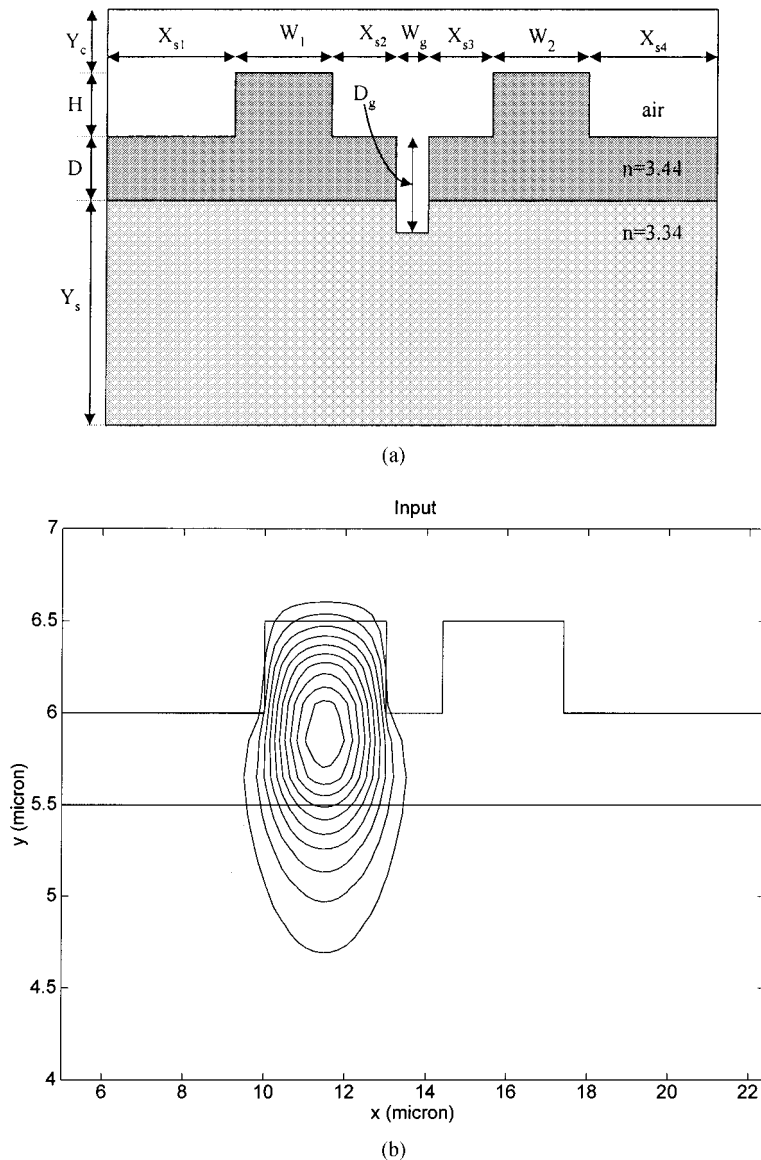


**Figure 1** (a) Cross-sectional view of the three-dimensional directional coupler structure with an etched-groove depth  $D_g$  and width  $W_g$  placed between the two rib waveguides. The common parameters used in the analysis are:  $Y_s = 5.5$ ,  $D = 0.5$ ,  $H = 0.5$ ,  $Y_c = 0.5$ ,  $X_{s1} = X_{s4} = 10.0$ ,  $W_1 = W_2 = 3.0$ , and a wavelength of 1.55 (all dimensions are in micrometers). (b) Field contours of the first guided mode of a single rib waveguide used as input in the study

coupling length of the directional coupler can be found as  $L_c = \lambda/2(n_e^{\text{eff}} - n_o^{\text{eff}})$ , where  $\lambda$  is the wavelength. For the structure of Figure 1, the coupling length is found to be  $L_c = 6500 \mu\text{m}$ . All of the results appearing in this study were computed using  $\Delta x = \Delta y = 0.1 \mu\text{m}$ ,  $\Delta z = 0.0275 \mu\text{m}$ , and zero field boundary condition at the edge of the computational window. The parameters of Figure 1(a) indicate that the modes of the rib waveguides are strongly confined; in addition, a large computational window has been used to minimize the influence of the zero fields at its edge. For the purpose of identifying the power loss due to the introduction of an etched groove in the structure, the normalized transmissivity of the left and right channels is evaluated during the

course of propagation. The computation of the normalized transmissivities has been carried out numerically by evaluating the square of the magnitude of the projected total BPM field  $\phi(x, y, z)$  onto the normalized mode  $\psi(x, y)$ , and then normalizing with respect to the input intensity, which can be expressed as

$$I_{\text{norm}}^{l,r}(z) = \left[ \left| \int_A \int \psi^{l,r} \phi^{l,r}(z) dA \right|^2 \right] / \left[ \int_A \int |\psi^{l,r}|^2 dA \int_A \int |\phi^l(0)|^2 dA \right] \quad (4)$$

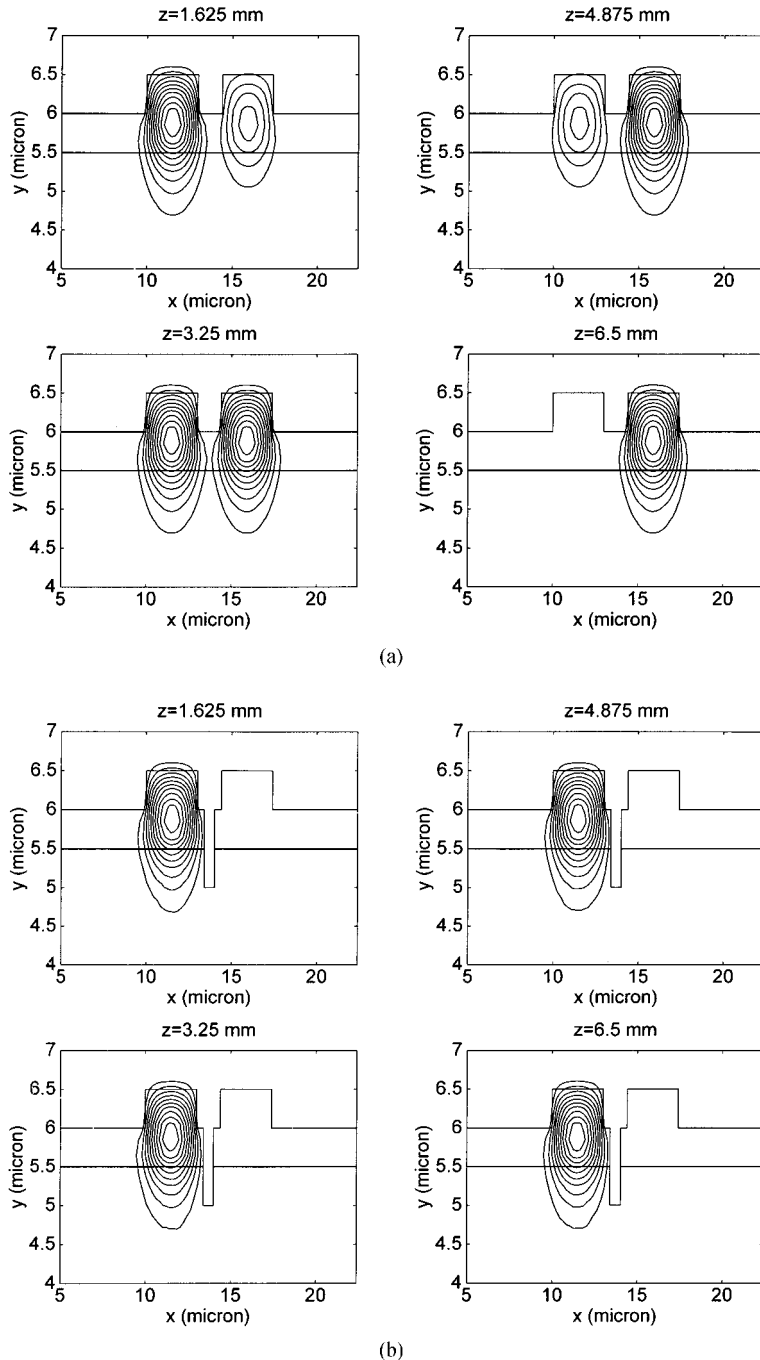


**Figure 2** (a) Field contours showing the power exchange between the two arms of the directional coupler of Figure 1 in the absence of etched groove ( $D_g = 0$ ) at several propagational distances. (b) Same as in (a), but with an etched groove of  $D_g = 1.0 \mu\text{m}$  and  $W_g = 0.6 \mu\text{m}$ , placed symmetrically ( $X_{s2} = X_{s3} = 0.4 \mu\text{m}$ ), showing the isolation of interaction between the two waveguides

where  $A$  is the cross-sectional area, and  $L$  and  $r$  represent the left or right waveguide, respectively.

**3.1. A Symmetric Etched Groove.** In this section, the study of a *symmetrical* etched groove introduced between the two waveguides is shown using different groove depth and width parameters. First, the results of the propagation of the field inside the structure of Figure 1(a) without an etched groove is evaluated. Figure 2(a) shows contour plots of the field for the power exchange between the two waveguides with  $D_g = 0$

at several propagational distances and an input field [of Fig. 1(b)] applied at  $z = 0$ . It is clear from the figure that complete coupling takes place at a length of  $z = 6500 \mu\text{m}$ , as predicted earlier. Figure 2(b) shows the same computation as in Figure 2(a), but with an etched groove of depth  $D_g = 1 \mu\text{m}$  introduced at  $z = 0$  right in the middle of the space (symmetrically) between the two waveguides. The action of the etched groove in isolating the waveguides is clearly demonstrated, where the power introduced into the left waveguide is seen to remain in this channel because of the

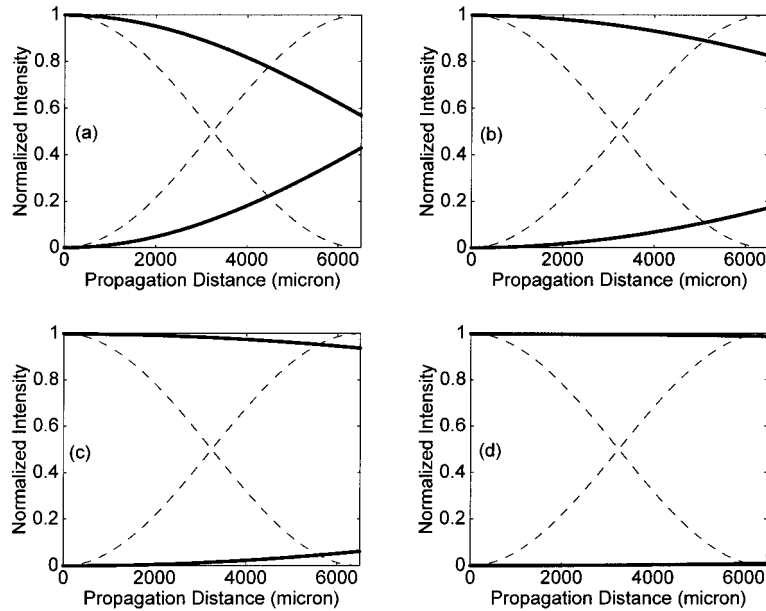


**Figure 3** Normalized intensities of the left and right waveguide fields during the course of propagation for several symmetrical groove depths  $D_g$ . Curves starting from 1 belong to the *left* waveguide where the input is applied, and curves starting from 0 belong to the *right* waveguide. Dashed curves are for  $D_g = 0$ , and solid curves are for  $W_g = 0.6 \mu\text{m}$  and (a)  $D_g = 0.2 \mu\text{m}$ , (b)  $D_g = 0.3 \mu\text{m}$ , (c)  $D_g = 0.4 \mu\text{m}$ , (d)  $D_g = 0.6 \mu\text{m}$ . Other parameters are the same as those used in Figures 1 and 2

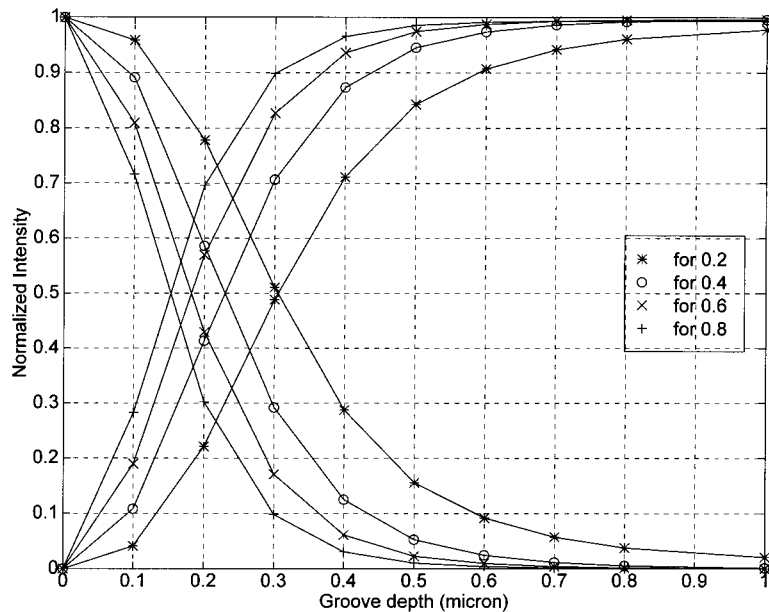


**Figure 4** Normalized intensities of the left and right waveguide fields at  $z = 6500 \mu\text{m}$  as a function of groove depth  $D_g$  for several groove widths  $W_g$  of a symmetric groove with  $X_{s2} + W_g + X_{s3} = 1.4 \mu\text{m}$ . Curves starting from 0 belong to the *left* waveguide where the input is applied, and curves starting from 1 belong to the *right* waveguide.  $W_g = 0.2$  (\* curves),  $0.4$  (o curves),  $0.6$  (x curves), and  $0.8$  (+ curves)  $\mu\text{m}$ . Other parameters are the same as those in Figure 1

existence of the groove. Figure 3 shows the normalized intensities of the left and right waveguides as a function of propagation distance for several groove depths. The zero groove-depth case has been included in the figure for comparison. It is clear from the figure that, as the groove depth increases, the interaction length between the two waveguides increases. For a groove depth of  $0.6 \mu\text{m}$  (and the structure at hand), the interaction between the two waveguides can be considered to be negligible. It is to be noticed that the power loss in the presence of a groove is also negligible. Figure 4 shows the normalized intensities of the left and right waveguide fields at the output of the structure ( $z = 6500 \mu\text{m}$ ) as a function of the groove depth  $D_g$  for several groove widths  $W_g$ . It is to be noticed again that the power loss due to the introduction of the etched groove is almost negligible. In addition, it is to be concluded that the way to increase the interaction length between the two waveguides is by increasing the width or depth of the etched groove or by increasing both parameters.

**3.2. An Asymmetric Etched Groove.** In this section, the study of introducing an *asymmetric* etched groove between the two waveguides of the directional coupler structure is shown. It is to be remembered that the distance between the two arms is kept constant ( $1.4 \mu\text{m}$ ). Figure 5 shows the normalized intensities of the left and right waveguides as a function of propagation distance for several asymmetrical parameters using  $W_g = 0.2$  and  $D_g = 0.3 \mu\text{m}$ . The zero groove-depth case and the symmetric case have been included in the figure for comparison. It is to be noticed that the results of Figure 5(a) and (b) are, respectively, for shifting the groove to the left and to the right by  $0.2 \mu\text{m}$  compared with the symmetrical case. Also, the results appearing in Figure 5(c) and (d) are, respectively, for shifting the groove to the left and to the right by  $0.4 \mu\text{m}$  compared with the symmetrical case. The figure shows the close agreement between the

results of shifting the groove to the right or left by the same distance. It is believed that the coupling lengths for both cases are equal to each other because the differences between the effective indexes of the even and odd super modes of the two cases are equal. Figure 6 shows the normalized intensities of the left and right waveguide fields at the output of the structure ( $z = 6500 \mu\text{m}$ ) as a function of the groove depth  $D_g$  for the same asymmetrical parameters of Figure 5. Generally, and compared with the symmetrical case, the asymmetrical structure produces a quicker isolation in the interaction between the two waveguides using fewer groove depths. Again, the isolation of the two waveguides in the asymmetrical case is accompanied by low power losses, which are always negligible.

#### 4. CONCLUSION

The characterization of isolating three-dimensional channel waveguides using an etched groove in the space between the two waveguides has been presented. The three-dimensional explicit finite-difference BPM was used successfully in the analysis. For optimization purposes, the variation of the parameters of the etched groove, the width, depth, and position of introducing the groove, have been studied carefully in the work. It is concluded that the technique of separating the interaction between two optical waveguides using the etched groove is generally very effective in terms of abruptness of action and low power loss. The optical interaction between the two channels is found to be very sensitive to the variation of both the width and depth of the groove. Also, the asymmetric etched grooves are more effective in the isolation of interaction than the symmetrical groove.

#### ACKNOWLEDGMENT

The support of King Fahd University of Petroleum and Minerals, Dhahran, Saudi Arabia, is gratefully acknowledged.

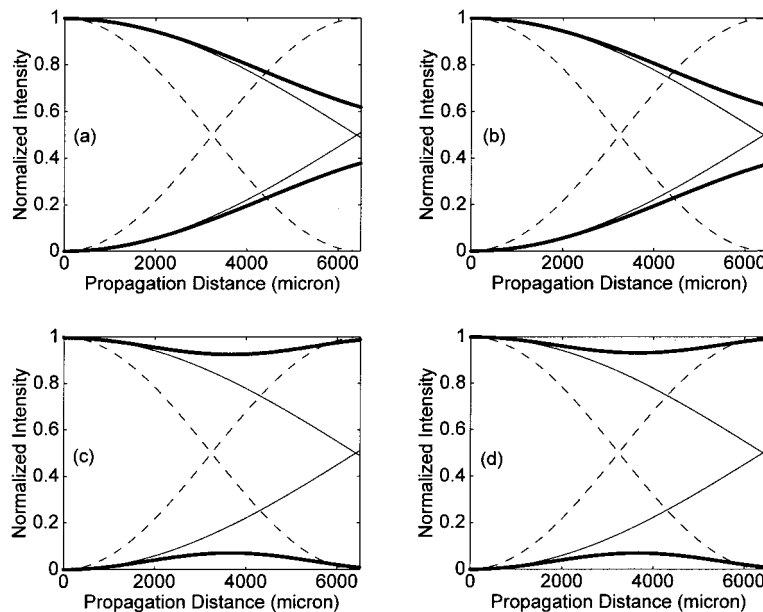


**Figure 5** Same as in Figure 3, with the addition of the asymmetric results, and with  $W_g = 0.2$ ,  $D_g = 0.3$ , and  $X_{s2} + W_g + X_{s3} = 1.4 \mu\text{m}$ . Dashed curves are for  $D_g = 0$ , solid curves are for symmetric groove ( $X_{s2} = 0.6$ ,  $W_g = 0.2$ ,  $X_{s3} = 0.6$ ) and **bold** solid curves are for asymmetric groove with (a) left-shifted  $X_{s2} = 0.4$ , (b) right-shifted  $X_{s2} = 0.8 \mu\text{m}$ , (c) left-shifted  $X_{s2} = 0.2$ , (d) right-shifted  $X_{s2} = 1.0 \mu\text{m}$

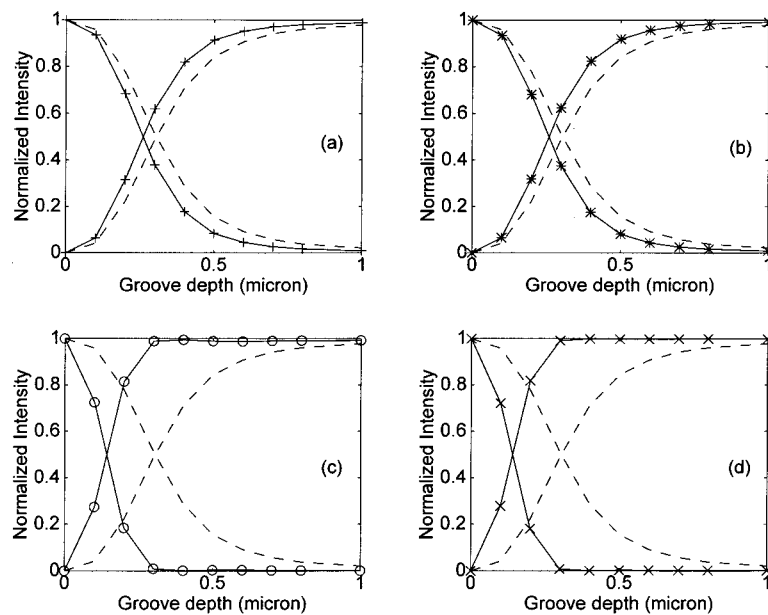


**Figure 6** Same as in Figure 4, with the addition of the asymmetric results, and with  $W_g = 0.2$ , and  $X_{s2} + W_g + X_{s3} = 1.4 \mu\text{m}$ . Dashed curves are for symmetric groove ( $X_{s2} = 0.6, W_g = 0.2, X_{s3} = 0.6$ ), and solid curves are for asymmetric groove with (a) left-shifted  $X_{s2} = 0.4$ , (b) right-shifted  $X_{s2} = 0.8 \mu\text{m}$ , (c) left-shifted  $X_{s2} = 0.2$ , (d) right-shifted  $X_{s2} = 1.0 \mu\text{m}$

## REFERENCES

1. S.J. Al-Bader, Application of etched grooves in integrated-optics channel isolation, *IEEE Photon Technol Lett* 8 (1996), 1044–1046.
2. H.M. Masoudi and S.J. Al-Bader, Three dimensional modeling of etched groove separation of adjacent optical waveguides, *Microwave Opt Technol Lett* 23 (1999), 289–291.
3. Y. Chung and N. Dagli, Analysis of Z-invariant and Z-variant semiconductor rib waveguides by explicit finite difference beam propagation method with nonuniform mesh configuration, *IEEE J Quantum Electron* 27 (1991), 2296–2305.
4. H.M. Masoudi and J.M. Arnold, Parallel three-dimensional finite-difference beam propagation methods, *Int J Numer Modeling* 27 (1995), 95–107.
5. H.M. Masoudi and J.M. Arnold, Modeling second-order nonlinear effects in optical waveguides using a parallel-processing beam propagation method, *IEEE J Quantum Electron* 31 (1995), 2107–2113.
6. M.D. Feit and J.A. Fleck, Computation of mode eigenfunctions in graded index optical fibers by the propagating beam method, *Appl Opt* 19 (1980), 2240–2246.

© 2000 John Wiley & Sons, Inc.

## MODELING OF METAL–SEMICONDUCTOR–METAL PHOTODETECTOR FOR SPICE

Jianjun Gao<sup>1</sup>, Baoxin Gao,<sup>1</sup> and Chunguang Liang<sup>2</sup>

<sup>1</sup> State Key Lab on Microwave & Digital Communication  
Tsinghua University  
Beijing 100084, P.R. China

<sup>2</sup> Hebei Semiconductor Research Institute  
050051, P.R. China

Received 21 March 2000

**ABSTRACT:** An equivalent circuit model for a metal–semiconductor–metal (MSM) photodetector based on microwave port characteristics is presented for a SPICE simulator. The experiential formulas of dc characteristics and intrinsic capacitance–voltage characteristics are given. The model parameters are obtained from dc and C–V measurement data by using curve fitting. Results are compared with experimentally obtained data, and excellent agreement is obtained consistently on MSM PDs of different sizes. © 2000 John Wiley & Sons, Inc. *Microwave Opt Technol Lett* 26: 390–394, 2000.

**Key words:** photodetector; device modeling; CAD

## INTRODUCTION

Metal–semiconductor–metal photodetector (MSM PDs) have attracted a great deal of attention for optoelectronic integrated circuits because of their high operating speed, ultra-low intrinsic capacitance, and compatibility with high-performance field-effect-transistor technology. These features are essential for building high-speed, high-sensitivity, wide-bandwidth OEIC receivers, which include monolithically integrated MSM PD and MESFET (HEMT) preamplifiers.

The modeling of an MSM PD is very useful for optoelectronic integrated circuit computer-aided design. Several approaches have been investigated for MSM PD modeling by numerically solving the device physical equation [1, 2]. This